Quench position reconstruction through harmonic field analysis in superconducting magnets

Quench Position Reconstruction through Harmonic Field Analysis in Superconducting Magnets

S Mariotto[1], M Sorbi[2]

[1] Istituto Nazionale di Fisica Nucleare, INFN - Laboratorio di Acceleratori e Superconduttività Applicata, Segrate, Italy
[2] Università degli Studi di Milano, Physics Department Aldo Pontremoli, Milano, Italy

E-mail: samuele.mariotto@mi.infn.it

May 2021

Abstract. The performances of superconducting magnets for particle accelerators are limited by instabilities or disturbances which lead to the transition of the superconducting material to the normal resistive state and the activation of the quench protection system to prevent damage to the magnet. To locate the position of the state transition, voltage taps or quench antennas are the most commonly used technologies for their reliability and accuracy. However, during the production phase of a magnet, the number of voltage taps is commonly reduced to simplify the construction process and quench antennas are generally used only for dipoles or quadrupoles to limit the antenna design complexity. To increase the accuracy in the reconstruction of the quench event position, a novel method, suitable for magnets with independent superconducting coils and quench protected without the use of quench heaters is proposed in this paper. This method, based on standard magnetic measurement techniques for field harmonic analysis, can locate the position of the superconductor transition inside the magnet after the quench event when the magnet has been discharged. Analyzing the not allowed harmonics produced in the field quality at zero current, the position of the quenched coils can be retrieved for any magnet orders without increasing the complexity of the dedicated measurement technique.

Submitted to: *Supercond. Sci. Technol.*

1. Introduction

Modern superconducting magnets, developed for particle accelerators, are designed to reach a working point as close as possible to the critical surface of the superconducting material and maximize their performances. Instabilities and disturbances of the superconducting coils when the magnet is powered [1], could cause the transition of the superconducting material to the normal resistive state and force the magnet discharge to prevent damage to the magnet. Even if the most important parameter for the quench protection is the delay time from the quench detection to the protection activation [2], also the location of the quench event is particularly interesting to evaluate if possible weak points of the superconducting coils are present in the magnet assembly. Considering superconducting magnets where the quench development is limited to one of the windings, the material which experienced the transition at the normal resistive state will not show a superconducting magnetization like the rest of the winding in the magnet. This asymmetry of the superconductor magnetization affects the residual magnetic field produced by the magnet at zero current and its quality is directly influenced by the position of the quenched coil in the magnet layout. The magnetic field quality can be measured after the quench event using standard magnetic field measurement techniques like rotating coils with high levels of accuracy and signal-to-noise ratio, [3]-[4]. In this paper, a first analytical model, considering the superconducting magnetization in the 2D magnet cross-section, is used to evaluate the expected magnetic field quality produced by the asymmetrical configuration and retrieve how the field quality can be directly linked to the quenched coil position. A 2D finite element (FE) model, used to improve the accuracy of the analytical model, is also presented and used to evaluate all the possible combinations of quenched coils configurations for the considered magnets. The comparison between simulations and measured magnetic field quality after real quench events of different magnets is also described in detail validating this new method as a powerful diagnostic system for modern superconducting magnets.

2. Analytical Description of Field Harmonics for superconducting magnetization after quench

After the current decay due to a quench event in a superconducting magnet, the magnetic field quality produced in the bore is the product of the weak field produced by persistent currents inside the coils still in the superconducting state and the residual magnetization of the iron. Especially if no quench heaters or induced coupling current technologies [5] are used for the magnet protection during a quench event, the winding not affected by the quench propagation can be modeled with a residual magnetization due to the superconductor persistent currents. Considering a 2D approximated model of a superconducting magnet, both the two magnetizations of the superconductor and the iron are functions of the powering cycle. The magnetized superconductor coil cross-section can be considered equivalent to a magnetization dipole in the 2D plane which direction and magnitude are functions of the field map of the magnet, see Figure 1. The magnitude can be calculated using the scalar Bean model [6] to evaluate the contribution of the strand residual magnetizations.

$$M = \frac{2}{3\pi} J_c D_s \frac{\lambda^{\frac{3}{2}}}{\sqrt{N_f}} \lambda_c \tag{1}$$

The value of the superconductor magnetization, obtained by the Equation 1 is obtained from the critical current density J_c flowing in the superconductor filaments area, the superconductor to strand volume ratio λ, the ratio λ_c between the area of all the strands and the whole coil area and the strand diameter D_s. Considering NbTi superconducting coils, the critical current density is usually fitted on measured data with different models which may diverge to infinity for very low magnetic fields. To retrieve the correct superconductor magnetization at zero current after the magnet discharge, the Kim-Anderson model [7]-[8], described by the following equation, can be used for low values of magnetic fields.

$$J_c(B) = \frac{J_0 B_0}{B + B_0} + A_0 + A_1 \cdot B \tag{2}$$

The values used in the model are reported in Table 1. Except for the ends of a superconducting magnet, the middle section of the coils produces a residual magnetization perpendicular to the magnet rotational axis. The two projections on the x and y-axis of the integrated magnetization over the coil volume can be then considered as magnetic moments with equivalent current loops I_1 and I_2 in the two x-y directions described by:

$$\begin{aligned} m_x &= I_1 dy Lz \\ m_y &= I_2 dx Lz \end{aligned} \tag{3}$$

where dx, dy identify the dipole dimentions and the parameter L_z defines the equivalent length of the

	J_0	B_0	A_0	A_1
Unit	A/mm^2	T	A/mm^2	A/Tmm^2
Value	2.02E+04	0.1203	5.97E+03	-7.0E+02

Table 1. Kim-Anderson Model Parameters

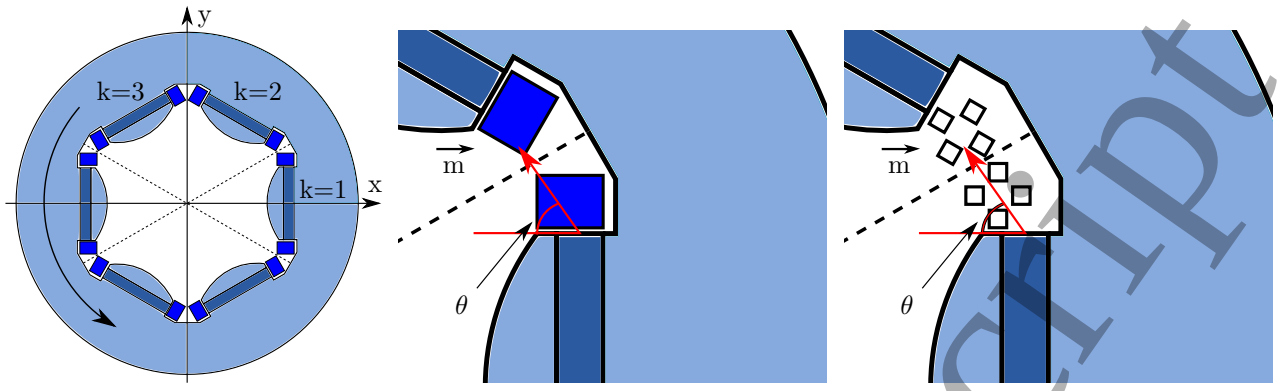

Figure 1. (*Left*) Superconducting magnet in a sextupolar symmetric configuration. (*Center* and *Right*) Equivalent representation of the magnetization dipole moment of the superconducting coil as model of current loops in the 2D magnet cross section plane

current loop in the magnet rotational axis direction. The contribution of these magnetic moments to the complex magnetic field harmonics can be calculated, according to [9], using the Equation 4

$$\mathrm{C}_n = \frac{i\mu_0}{2\pi}\int \frac{J}{w^n}d\sigma, \qquad \int J d\sigma = I \tag{4}$$

where $w = x + iy$ is the central position of the current loop cross-section in the complex 2D plane and J its current density. To describe the arbitrary magnetization dipole orientation, the two m_x and m_y projections on the magnet reference frame can be calculated separately and added together as reported in Equation 5.

$$\begin{aligned}\mathrm{C}_n = \frac{i\mu_0}{2\pi}\int \mathrm{d}\sigma\ \frac{J_1}{\left(w-\frac{i\mathrm{d}y}{2}\right)^n} - \frac{J_1}{\left(w+\frac{i\mathrm{d}y}{2}\right)^n} \\ + \frac{i\mu_0}{2\pi}\int \mathrm{d}\sigma\ \frac{J_2}{\left(w+\frac{\mathrm{d}x}{2}\right)^n} - \frac{J_2}{\left(w-\frac{\mathrm{d}x}{2}\right)^n}\end{aligned} \tag{5}$$

The ratio between the dipole magnetization dimensions (dx,dy) and w is much lower than the single unit allowing the Taylor expansion approximation at the first order of the fractions. With some algebra we can obtain the Equation 6

$$\begin{aligned}\mathrm{C}_n &= \frac{i\mu_0 n}{2\pi}\int \mathrm{d}\sigma \left[\frac{J_1 i\mathrm{d}y}{w^{n+1}} - \frac{J_2 \mathrm{d}x}{w^{n+1}}\right] \\ &= -\frac{\mu_0 n}{2\pi L_z}\left[\frac{m_x + i m_y}{w^{n+1}}\right]\end{aligned} \tag{6}$$

The current density and the transversal dimension of the magnetization dipole can be collected in the cartesian components of the dipole module described in the 2D complex plane. Considering a single superconducting coil in symmetrical configuration to the x-axis, see Figure 2, for a magnet with 2b poles, if the transversal length is much lower of the magnet aperture where the field is evaluated, the two m_x and m_y components of the two cross-sections which

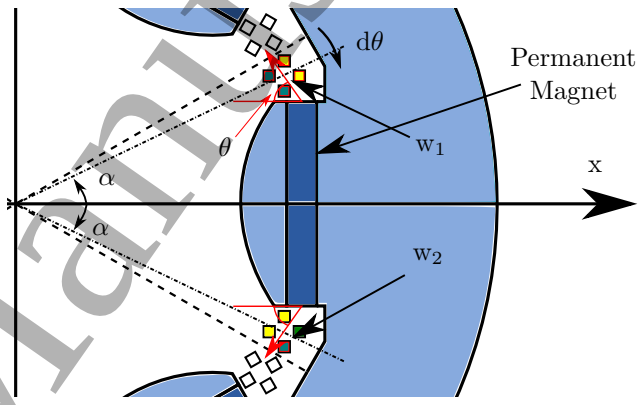

Figure 2. Details of the superconducting coil magnetization dipole moments. The parameters used in the analytic model are reported in the figure and the two cross sections of the superconducting coil are highlighted

contribute to the harmonic coefficients can be identified by the two central positions w_1 and w_2 with the same module ρ and an aperture angle α. Since we made the hypothesis that the considered superconducting coil has an up-down symmetry, the magnetization orientations of the two coil cross-sections are reversed in the y-axis $m_1 = m_x + i m_y$ and $m_2 = m_x - i m_y$ leading to the two contributions to the harmonic coefficients reported in Equation 7.

$$\begin{aligned}\mathrm{C}_n^1 &= -\frac{\mu_0 n}{2\pi L_z}\left[\frac{m_1}{w_1^{n+1}}\right] = -\frac{\mu_0 n}{2\pi L_z}\left[\frac{m_1}{\rho^{n+1}}\right] e^{-i(n+1)\alpha} \\ \mathrm{C}_n^2 &= -\frac{\mu_0 n}{2\pi L_z}\left[\frac{m_2}{w_2^{n+1}}\right] = -\frac{\mu_0 n}{2\pi L_z}\left[\frac{m_2}{\rho^{n+1}}\right] e^{i(n+1)\alpha}\end{aligned} \tag{7}$$

The coil aperture angle α can be written as $\alpha = \frac{\pi}{2b} - \mathrm{d}\theta$, where the integer b identifies the geometrical magnet rotational symmetry in which each pole have an aperture of $\frac{2\pi}{2b}$ degrees and the parameter $\mathrm{d}\theta$ represents the coil cross-section angular distance from the symmetry axis between two consecutive magnetic poles. By adding the two harmonic coefficients in Equation 7 the obtained

function describes the total contribution of a single full magnetized superconducting coil. This magnetic field harmonics contribution can be extended to consider all the k^{th} superconducting coils by rotating the magnetization dipole moments of an angle $(k-1)\pi/b$.

$$m_1 \rightarrow m_1^{'} = m_1\ (-1)^{k-1}\ e^{i(k-1)\frac{\pi}{b}}$$
$$m_2 \rightarrow m_2^{'} = m_2\ (-1)^{k-1}\ e^{i(k-1)\frac{\pi}{b}} \quad (8)$$

With k limited to the range $[1, 2b]$. To account for the polarity of every single coil in the magnet and invert the magnetized dipole orientation, the scaling factor $(-1)^{k-1}$ is used. Considering that the cross-section position of the magnetic dipole moments w_1 and w_2 are transformed applying a rotating angle of $(k-1)\pi/b$, the expression for the harmonic coefficients produced by the generic k^{th} coil is reported in Equation 9.

$$\mathrm{C}_n(k) = \frac{-\mu_0 n}{2\pi L_z \rho^{n+1}} \left[m_1 e^{-i(n+1)\alpha} + m_2 e^{i(n+1)\alpha} \right] \cdot e^{i\pi(k-1) - in(k-1)\frac{\pi}{b}} \quad (9)$$

The m_2 dipole, due to the up and down symmetry, can be rewritten as the complex conjugate of m_1. Therefore, in the previous equation, the values in the square bracket compose the real part of the first addendum with phase angle of α. In addition, the magnetization dipole m_1 can be written as function of its magnitude m and the orientation angle θ from the x-axis of the magnet frame obtaining the Equation 10.

$$\mathrm{C}_n(k) = \frac{-\mu_0 n m}{2\pi L_z \rho^{n+1}} \cos[\theta - (n+1)\alpha] e^{-i\frac{n-b}{b}(k-1)\pi} \quad (10)$$

The amplitudes of the harmonic coefficients, independently from the considered magnetized coil, are proportional to the magnetization dipole amplitude and depend both on the dipole orientation θ and the coil angle α. The phase of every single harmonic coefficient, instead, is a function of the magnetized coil and is shifted by the quantity $\frac{n-b}{b}\pi$. Looping through all coils of the superconducting magnet, the overall magnetic field quality is calculated using Equation 11 where we considered that only the j coil has quenched.

$$\mathrm{C}_n^j = \sum_{k=1}^{2b} \mathrm{C}_n(k) - \mathrm{C}_n(j) \quad (11)$$

The first sum of the harmonic coefficients is null for all the harmonic orders not allowed in a classical b order magnet. In a $2b$-order magnet with a full symmetrical configuration, the only allowed harmonics are the odd multiples of b. Here, we call the "not-allowed harmonics the magnetic field components which should not be present considering the symmetry of the analyzed magnet. The only term which generates not allowed harmonics is due to the single quenched coil contribute described by the Equation 10. Comparing the not allowed harmonics, fixed the magnet order, the harmonic coefficients with orders $n = b \pm 1$ allow a unique reconstruction of the single quenched coil. The same pattern, with different intermediate phases of the harmonic coefficients, is obtained if two or more coils are quenched allowing also the reconstruction of multi-coils quench events in the magnet training.

3. FE Model for superconducting magnetization analysis

The previously described analytic model, used to evaluate the harmonic coefficients of the magnetic field quality produced after a quench, does not take into account the presence of the iron in the magnet cross-section. The magnetic field produced by the superconducting coil magnetization is deformed by the iron laminations of the magnet and the harmonic contents resulting depends on the iron pole shape and external iron yoke dimensions. To evaluate the real deformation of the iron laminations on the magnetic field path, a hysteretic behavior has to be taken into account depending on the powering cycle performed on the magnet. Superconducting magnets for particle accelerators are assembled with low carbon magnetic steel for its negligible coercivity and permeability values. This requirement is needed to assure that the same magnetic field is provided to the accelerated particles and predict the magnet behavior during the powering. The superconductor magnetization, considered in the analytical model, creates a small magnetization effect of the iron lamination due to the small contribution to the applied magnetic strength on the iron and can be therefore neglected if compared to the iron residual magnetization due to the hysteretic behavior and provoked during the powering cycle. A complete model of the iron hysteretic behavior is generally difficult to be obtained without a dedicated measuring campaign being a varying function of the iron quality and thermal cycles used during the production phase. To model the hysteretic behavior of the iron without the use of a complex model, which would have to be validated on real data, we reproduced its contribution to the field quality with an equivalent permanent magnet in the FE model. The parameters used for the permanent magnet, like its thickness and BH curve, have been tuned to reproduce previously measured values of field flux and magnetic field quality created by the magnet after a slow ramp down at zero current. The superconductor magnetization in the FE model has been simulated with the same approximation adopted for the analytical calculation. Each coil is represented by a magnetization dipole with a magnitude equivalent to the all coil cross-section magnetization amplitude and the same orientation as the average magnetic field map on the cross-section center. As expected, the main harmonic component of

the produced magnetic field in the 2D FEM simulation is dominated by the iron magnetization, and the not allowed harmonics are not affected by the iron presence. This effect is due to the iron magnetization which is due to the powering cycle and creates only the allowed harmonics for the symmetry of the iron shape.

4. Examples of analysis in superconducting magnets

The previously described model has been tested on real quench events of the High Order Corrector magnets prototype and production series during the powering test performed at LASA laboratories in Milan, Italy. The High Order (HO) corrector magnets development has been entrusted to the LASA superconducting magnet group department for the next upgrade project of LHC called High Luminosity LHC "HiLumi-LHC", [10]. The upgrade project will provide up to 10 times the integrated luminosity of the nominal modern value to increase the acquired particle collisions statistic from the detectors and improve the discovery power of the collider for the next years. The new superconducting magnet string in the Interaction Regions (IR) is only one of the different key technologies that will be installed together in 2025. The High Order superconducting corrector magnets are divided into five types based on different rotational orders of symmetry from quadrupole up to the dodecapole configuration and their strength has been designed to be able to compensate the beam instabilities caused by the field errors in the main low-β quadrupole and recombination dipole of the string [11]. The superferric design of these magnets [12]-[14], in which the magnetic field of the n separated superconducting coil is shaped by the iron poles geometry to produce the required quality, is characterized by a limited quench propagation to some of the superconducting windings

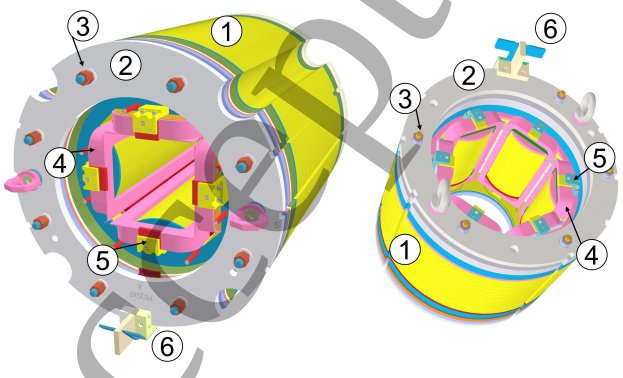

Figure 3. Sketch 3D of the MQSXFP1 and MCSXF corrector magnets showing the main components: 1 -Iron laminations, 2 - Stainless steel plate, 3 - CuBe tie-rods, 4 - Superconducting NbTi coils, 5 - Coil support, 6 - Current leads.

leaving the not quenched coils still magnetized after the magnet discharge. The quench propagation inside the superconducting coils has been already studied and characterized during the development of the first magnet prototypes for any magnet order. In the early phase of prototyping, [15]-[18], every single superconducting coil had been instrumented with voltage taps showing no propagation of the quench between near windings inside the magnet. Later, for the series production, only the "middle" voltage taps have been maintained in magnets and used to detect the transition by comparison of the two halves of the whole superconducting winding to retrieve only the quench resistive voltage.

4.1. Magnetic Measurement

The characterization of the produced magnetic field quality of the HO corrector magnets, has been performed using a standard rotating coil measurement technique. A complete new measurement system, developed by the CERN Magnetic Measurement department, has been installed in the vertical cryogenic magnet test station at the LASA laboratory. The data acquisition hardware is composed of a patch panel connected to the voltage taps of the rotating coils, 2 fast digital integrators (FDIs) which analyze the induced voltage, and a 512 steps angular encoder and the motor unit which provide the motion to the shaft and control the rotational speed equal to 1 Hz. The rotating shaft used for the magnets test, see [19], is a 1.5 m long carbon fiber rotating shaft that mounts a 5 radial coils PCB. The reference measuring radius of the external radial coil on the PCB is equal to 45 mm so the measured field quality is then extrapolated at 50 mm which corresponds to the reference radius of the magnets. The induced voltage on the PCB coils is produced by the rotation inside the magnet and is sampled by the FDIs which convert the signal to the equivalent magnetic field flux on the coil surface area precisely calibrated before the measurement. The magnetic field calculated after the conversion is then analyzed through a Fast Fourier Transform to retrieve the harmonic coefficients of the magnet field quality as a function of the magnet operating current.

4.2. Quadrupole MQSXFP1 Quench Localization

The first magnet analyzed with our method is the quadrupole MQSXFP1 [20] during the second and third assemblies (MQSXFP1b and MQSXFP1c) tested in July and October 2020 at LASA together with the other magnets of the series production [21],[22]. During the training phase, the MQSXFP1c magnet had 7 different quenches before reaching the ultimate current and all the quench events have been checked by the

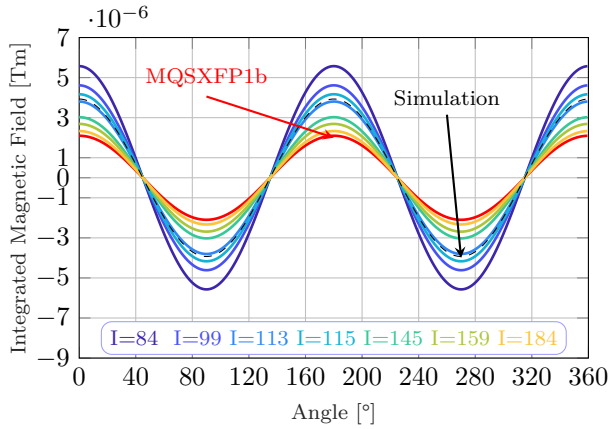

Figure 4. Quadrupolar component of the magnetic field measured after quench events of MQSXFP1c.

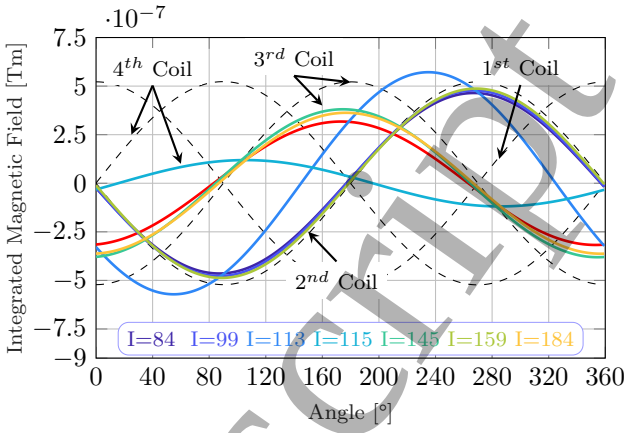

Figure 5. Dipolar component of the magnetic field measured after quench events of MQSXFP1c.

quench detection system analyzing the two halves (A or B) of the magnet to determine where the quench occurred. Only the 4^{th} quench event, developed at I= 115 A, has been recorded as developed in the B side of the magnet while all the other quench have been recorded in the A-side. Using the Fourier transform of the magnetic field total flux taken from each single quench event, the single harmonic coefficients have been obtained and compared with quench event simulations. In the following figures, we reported for comparison the dipolar, quadrupolar, and sextupolar harmonics of the magnetic field flux after quench events. As we expected, all the quadrupolar harmonic components of the analyzed residual field flux have the same initial phase, see Figure 4. From the harmonic analysis, a small rotation of the main produced field has been observed, not evident in the plot, which is probably due to the accuracy of the alignment between the magnetic field measurement system and the magnet mechanical reference frame in the vertical cryostat. A dependence of the main field harmonic amplitude from the values of the current at which the quench occurred has been also observed in this assembly confirming the same behavior of MQSXFP1b where the iron contribution to the main field harmonic decreases with faster current decay rates. The measurements after the quench events, have been also classified in four main groups according to the results of the harmonic analysis performed on both the dipolar harmonic, Figure 5, and the sextupolar harmonic, Figure 6. All the colored lines reported represent the measured signal after each quench event while the dashed lines are obtained from the calculated harmonic component. The first group is composed of the quench events that occurred at I= 84 A, 99 A, and 159 A. The different signals have all the amplitude and the same initial phase which is compatible with a calculated quench event in the 1^{st} coil, see Figure 7. The

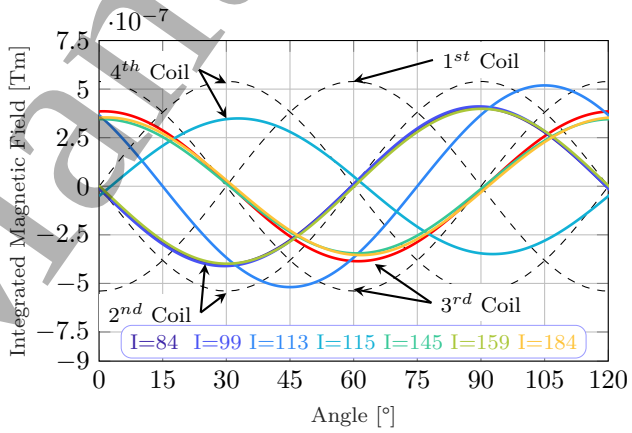

Figure 6. Sextupolar component of the magnetic field measured after quench events of MQSXFP1c.

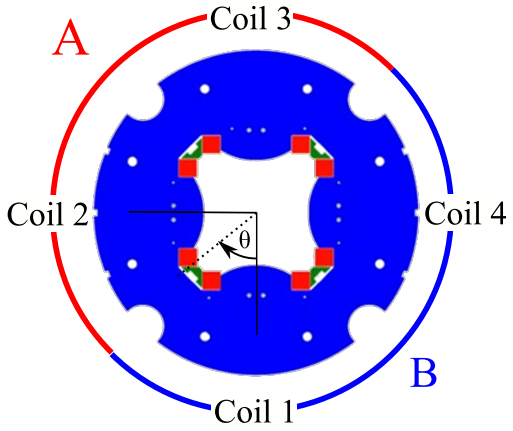

Figure 7. Sketch of the MQSXFP1 cross-section with highlighted the two halves A and B and the numbered superconducting coils.

second group, compatible with the calculated quench in the 2^{nd} coil, contains the two quench events at I= 145 A and 184 A. The same signal has been also obtained during the quench event that occurred in the MQSXFP1b assembly during its powering test. The third group is composed only by the quench event at I=115 A and the measured signal has the same phase value of the calculated quench event in the 3^{rd} coil of the magnet. Both the 1^{st} and 2^{nd} coil of the assembly belong to the A half of the magnet confirming the results measured by the fast acquisition of the QDS. The third group, instead, is being registered in the 3^{rd} coil of the assembly which belongs to the B side of the magnet, is also compatible with the QDS results. The fourth group contains only the quench that occurred at I=113 A. The harmonics of the residual flux, produced by this quench, have not a defined phase as predicted by the harmonic model both in the dipole and sextupole harmonic analysis. This quench event signal has an intermediate phase value between the one corresponding to the 1^{nd} and 2^{th} coil. Since both these coils belong to the half part of the magnet where the quench has been detected by the QDS system, the intermediate value of the phase identifies the development of this quench event in the same A-side of the magnet. The possible hypotheses to explain this not predicted harmonic content are for example an asymmetry of the quench propagation inside the superconducting coil, not considered in the analytical and FE model, which would have caused an asymmetric distribution of the residual superconductor magnetization and therefore an intermediate value of the predicted phase, or a transition of two or more coils which would lose their residual magnetization during the quench development and also explain the higher amplitude of the produced not allowed field harmonic components.

4.3. Sextupole MCSXF01 Quench Localization

The second magnet which has been characterized with the magnetic measurement system is the first sextupole produced for the HQ corrector series, MCSXF01. During the training of the first sextupole of the production series, only 5 quenches have been observed before reaching the ultimate current. All the quench events happened during the energization phase while the last quench, recorded to develop at the current of 112 A, happened during the one-hour stability test with inverse polarity. The same analysis previously described for MQSXFP1 has been performed also on the residual magnetic field incremental flux of the measured signals after the quench events. For the analysis of this magnet, the quadrupolar, sextupolar, and octupolar components of the magnetic field have been retrieved. The analysis of the main sextupolar harmonic, reported in Figure 8 shows that all the signals have roughly the same amplitude and initial phase. All the initial phases are compatible with the null value (or with half rotation for the I=112 A signal) within the error bar of the measurement while the main difference in the amplitude of the signals is a higher value for the 112 A quench event which is only produced in the main field harmonic. By considering the value of the initial phase, the analysis of the main harmonic can be also used to cross-check the polarity of the magnet during the energization test. Indeed all the training quench events happened during the positive energizing of the magnet, while the one-hour stability test has been performed at -I_{ult} giving, therefore, an opposed initial phase in the main harmonic generated after the last quench of the magnet. The quadrupolar

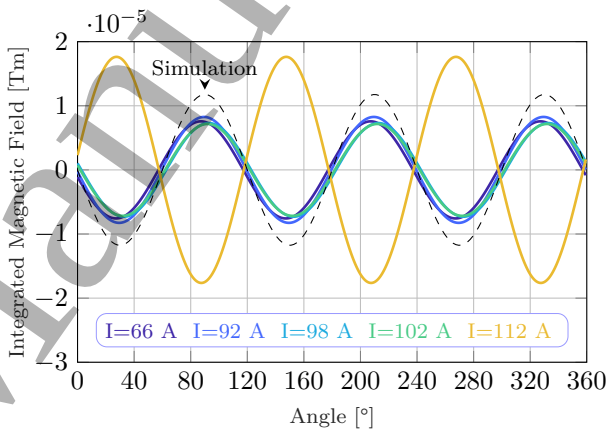

Figure 8. Main harmonic produced in the signal of MCSXF01 after quench events at zero current.

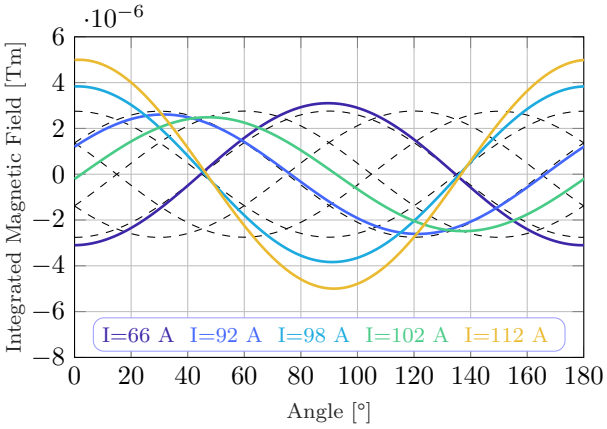

Figure 9. Representation of the reconstructed quadrupolar component of the magnetic field harmonic measured in the residual signal of MCSXF01 after quench events.

harmonic of the residual magnetic field produced after the quench events are reported in Figure 9. From the observation of the different curves, we can point out

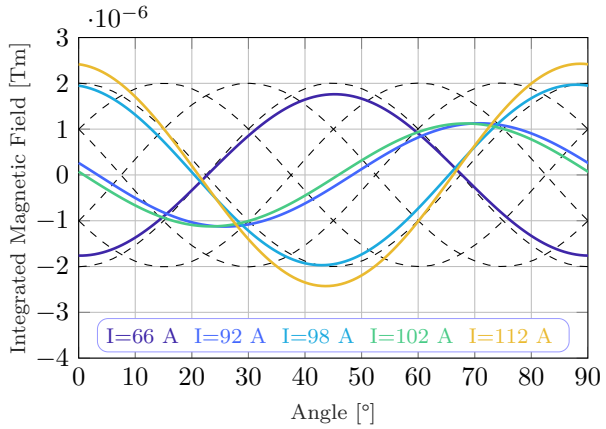

Figure 10. Octupolar component of the harmonics produced by MCSXF01 after each quench event.

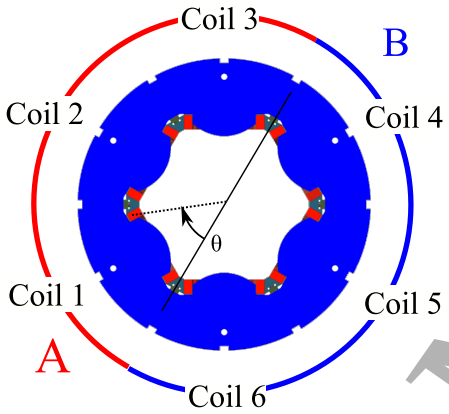

Figure 11. Sketch of the MCSXF cross-section with highlighted the two halves A and B and the numbered superconducting coils.

that the signals obtained from quench happened at I=112 A and 98 A have the same phase while the quenched at I=66 A has the opposite initial phase. These two different initial phases are predicted by the analytical and FE model of the magnet and are associated to a quenched coil at ±90° from the zero of the measurement (2^{nd} and 5^{th} coil, see Figure 11) if the magnet is in the normal configuration. Combining this information with the corresponding main harmonic component previously described, we reconstructed that the quenched happened at I=66 A and 112 A are localized in the B side of the magnet and more precisely are due to the same superconducting coil in the middle of the B side while the quench at I=98 A is localized in the A-side and is due to the superconducting coil in the middle. The quench event that occurred at I=92 A has instead an initial phase corresponding to the first coil which is reconstructed by the model in the A-side of the magnet. The same reconstruction and identified groups for all the quench events presented until now could also be performed observing the octupolar harmonic reported in Figure 10. All the reconstructions of the quenched coil position are perfectly matched from the QDS system which, however, is able only to localize the quench in the A or B side of the magnet. The only quench event, which generated a quadrupolar harmonic not predicted by the model is the one that happened at I=102 A. From the analysis of the measured initial phase of this event and the calculated model, the possible quenched coils, which produced the signal, are located immediately before and after the zero of the magnet reference system (1^{st} and 6^{th} coils in Figure 1 which are also corresponding to the position of the external connection of the magnet). To evaluate which one of the superconducting coils has quenched in the magnet we can observe the other calculated harmonic like for example the octupolar component of the magnetic field, reported in Figure 10. The quenched occurred at I=102 A has produced an octupolar magnetic field harmonic predicted by the model compatible also with the result obtained for the quench at I=92 A. From the observation of the harmonic model prediction, the quench position for these two events has been calculated to be in the 1^{st} coil of the A-side of the magnet in perfect agreement with the QDS system.

5. Conclusions

The method presented in this article describes the possibility to reconstruct after a quench the portion of the magnet which experienced the superconducting to the normal phase transition. The direct correlation between the measured magnetic field quality with the quenched configuration of the superconducting coils has been firstly reconstructed analytically with some basic approximations and then fully analyzed with Finite Element Method simulations. The comparison between simulated quench event configurations and real data, taken from two different types of the High Order Corrector magnets for the High Luminosity LHC upgrade project, shown a very good quench location reconstruction validating this analysis method. The position of the quenched coil has been precisely measured in the magnet bore allowing an improved sensibility, if compared to the resolution of the Quench Detection system, to every single superconducting coil installed in the magnet. From the analysis of the quench event, a random distribution of the quench event in the different coils of the HO corrector magnets has been observed showing no weak points or degraded winding. The presented method could be in principle applied not only to magnets with high order rotational symmetries as in our examples but also to conventional small length model of superconducting dipoles and

quadrupoles where no complete transition of the all superconducting coils is observed and segmented rotating coils can be used to study separately the coils straight section and the coil ends training behavior.

Acknowledgments

The results obtained in this paper would not have been possible without the help of the CERN Magnetic Measurement Department. In particular, the authors would like to thank the Magnetic Measurement of Superconducting Magnets group for gently providing the rotating coil shaft, the data acquisition framework, the motor control unit and the help during the hardware setup at the LASA cryogenic test station facility.

References

[1] M. N. Wilson. *Superconducting Magnets*. Clarendon Press, Oxford, U.K., Mar 1987.

[2] K. H. Mess. Quench Propagation and Magnet Protection. *Handbook of Applied Superconductivity, B. Seeber*, 1:527, 1998.

[3] L. Bottura and K. N. Henrichsen. Field Measurements. page 35 p, December 2002.

[4] L. Walkiers. Magnetic Measurement with Coils and Wires. In *CERN Accelerator School: Course on Magnets*, 4 2011.

[5] E. Ravaioli. *CLIQ. A New Quench Protection Technology for Superconducting Magnets*. PhD thesis, University of Twente, June 2015.

[6] C. P Bean. Magnetization of Hard Superconductors. *Physical Review Letters*, 8(6):250–253, 1962.

[7] Y. B. Kim, C. F. Hempstead, and A. R. Strnad. Critical Persistent Currents in Hard Superconductors. *Phys. Rev. Lett.*, 9:306–309, October 1962.

[8] P. W. Anderson. Theory of Flux Creep in Hard Superconductors. *Phys. Rev. Lett.*, 9:309–311, October 1962.

[9] G. Ambrosio and G. Bellomo. Magnetic Field, Multipole Expansion and Peak Field in 2D for Superconducting Accelerator Magnets. Technical Report INFN-TC-96-15, INFN, Rome, October 1996.

[10] L. Rossi and O. Bruning. High Luminosity Large Hadron Collider, The New Machine For Illuminating The Mysteries Of Universe. *Advanced Series On Directions In High Energy Physics, World Scientific Publishing Company*, 2015.

[11] E. Todesco, H. Allain, G. Ambrosio, G. Arduini, F. Cerutti, R. De Maria, L. Esposito, S. Fartoukh, P. Ferracin, H. Felice, R. Gupta, R. Kersevan, N. Mokhov, T. Nakamoto, I. Rakno, J. M. Rifflet, L. Rossi, G. L. Sabbi, M. Segreti, F. Toral, Q. Xu, P. Wanderer, and R. Van Weelderen. A First Baseline for the Magnets in the High Luminosity LHC Insertion Regions. *IEEE Transactions on Applied Superconductivity*, 24(3), 2014.

[12] G. Volpini, F. Alessandria, G. Bellomo, F. Broggi, A. Paccalini, D. Pedrini, A. Leone, M. Quadrio, L. Somaschini, M. Sorbi, M. Todero, C. Uva, P. Fessia, E. Todesco, and F. Toral. NbTi Superferric Corrector Magnets for the LHC Luminosity Upgrade. *IEEE Transactions on Applied Superconductivity*, 25(3):1–5, June 2015.

[13] G. Volpini, F. Alessandria, G. Bellomo, F. Broggi, A. Paccalini, D. Pedrini, A. Leone, V. Marinozzi, M. Quadrio, M. Sorbi, M. Statera, M. Todero, C. Uva, P. Fessia, A. Musso, E. Todesco, and F. Toral. Development of the superferric sextupole corrector magnet for the lhc luminosity upgrade. *IEEE Transactions on Applied Superconductivity*, 26(4):1–4, 2016.

[14] M. Sorbi, F. Alessandria, G. Bellomo, F. Broggi, A. Leone, V. Marinozzi, S. Mariotto, A. Musso, A. Paccalini, D. Pedrini, M. Quadrio, M. Statera, M. Todero, E. Todesco, and C. Uva. Status of the Activity for the Construction of the HL-LHC Superconducting High Order Corrector Magnets at LASA-Milan. *IEEE Transactions on Applied Superconductivity*, 28(3):1–5, 2018.

[15] M. Statera, F. Alessandria, F. Broggi, A. Leone, S. Mariotto, A. Paccalini, D. Pedrini, M. Quadrio, M. Sorbi, M. Todero, C. Uva, R. Valente, P. Fessia, A. Musso, and E. Todesco. Construction and Cold Test of the Superferric Decapole for the LHC Luminosity Upgrade. *IEEE Transactions on Applied Superconductivity*, 29(5):10–14, 2019.

[16] M. Sorbi, F. Alessandria, G. Bellomo, F. Broggi, M. Campaniello, M. Canetti, A. Fumagalli, F. Gangini, A. Leone, S. Mariotto, A. Musso, A. Paccalini, A. Pasini, D. Pedrini, M. Quadrio, M. Statera, M. Todero, E. Todesco, R. Valente, C. Uva, and A. Zanichelli. Construction and Cold Test of the Superferric Dodecapole High Order Corrector for the LHC High Luminosity Upgrade. *IEEE Transactions on Applied Superconductivity*, 29(5):1–5, 2019.

[17] M. Statera, F. Alessandria, F. Broggi, A. Leone, V. Marinozzi, S. Mariotto, A. Paccalini, D. Pedrini, M. Quadrio, M. Sorbi, M. Todero, C. Uva, P. Fessia, A. Musso, and E. Todesco. Construction and Cold Test of the Superferric Octupole for the LHC Luminosity Upgrade. *IEEE Transactions on Applied Superconductivity*, 28(4):14–18, 2018.

[18] M. Statera, G. Volpini, F. Alessandria, G. Bellomo, F. Broggi, A. Paccalini, D. Pedrini, A. Leone, V. Marinozzi, M. Quadrio, M. Sorbi, M. Todero, C. Uva, P. Fessia, A. Musso, E. Todesco, and F. Toral. Construction and Cold Test of the First Superferric Corrector Magnet for the LHC Luminosity Upgrade. *IEEE Transactions on Applied Superconductivity*, 27(4):1–5, 2017.

[19] L. Fiscarelli, H. Bajas, F. Mangiarotti, A. Musso, S. Russenchuck, S. Mariotto, M. Sorbi, and M. Statera. Magnetic Measurements on the Prototype Magnets of the High-Order Correctors for HL-LHC. *IEEE Transactions on Applied Superconductivity*, 29(5), 2019.

[20] M. Statera, F. Alessandria, G. Bellomo, F. Broggi, A. Leone, S. Mariotto, A. Paccalini, A. Pasini, D. Pedrini, M. Prioli, M. Sorbi, M. Quadrio, R. Valente, M. Todero, C. Uva, A. Musso, E. Todesco, M. Campaniello, M. Canetti, F. Gangini, P. Manini, and A. Zanichelli. Construction and Power Test of the Superferric Skew Quadrupole for HL-LHC. *IEEE Transactions on Applied Superconductivity*, 30(4), 2020.

[21] M. Prioli, F. Broggi, M. Campaniello, M. Canetti, E. De Matteis, F. Gangini, L. Imeri, A. Leone, P. Manini, S. Mariotto, A. Musso, A. Paccalini, A. Palmisano, A. Pasini, D. Pedrini, C. Santini, M. Sorbi, M. Statera, M. Todero, E. Todesco, C. Uva, R. U. Valente, and A. Zanichelli. Completion of the Test Phase for the Hilumi LHC Skew Quadrupole Corrector Magnet. *IEEE Transactions on Applied Superconductivity*, 31(5):1–5, 2021.

[22] M. Statera, F. Alessandria, G. Bellomo, F. Broggi, L. Imeri, A. Leone, S. Mariotto, A. Paccalini, A. Pasini,

D. Pedrini, M. Prioli, M. Sorbi, M. Todero, C. Uva, R. U. Valente, A. Musso, E. Todesco, M. Campaniello, M. Canetti, F. Gangini, P. Manini, C. Santini, and A. Zanichelli. Optimization of the High Order Correctors for HL-LHC Toward the Series Production. *IEEE Transactions on Applied Superconductivity*, 31(5):1–5, 2021.